Comparison of Sheared Granular Soils: Same Void Ratio but Considerably Different Fabric

Y. Fukumoto[1] and S. Ohtsuka[1]
[1]*Department of Civil and Environmental Engineering, Nagaoka University of Technology, Niigata, Japan*
E-mail: yfukumoto@vos.nagaokaut.ac.jp

ABSTRACT: This paper reports a comparison of two types of sheared granular soil specimens, with almost the same void ratios but considerably different fabric, using the discrete element method in two dimensions. The specimens are prepared by applying two different methods of particle generation; one specimen is generated by placing the particles geometrically, while the other specimen is generated by placing the particles randomly. Then, computational direct shear tests are conducted in order to compare the yielding behaviours of the two specimens. The obtained bulk shear responses show different trends, even though the values for the void ratio at the initial state are almost the same. Toward the critical state, however, the initial differences in the stress state and the granular fabric gradually disappear and eventually reach almost the same state. The results reveal that not only macroscopic quantities, but also the contact force distribution and the angular variation in contact forces, have a unique critical state. In particular, the angular distribution of contact angles inside the shear band is also found to have a unique critical state.

Keywords: Granular materials, Discrete element method, Shear behaviour

1. INTRODUCTION

There is considerable interest in the properties of the initial packing of granular materials, which depend on the packing conditions (Rothenberg and Bathurst, 1992; Jaeger et al., 1996; Mueth et al., 1998; Makse et al., 2000; Matuttis et al., 2000; Roux, 2000; Geng et al., 2001; Goldenberg and Goldhirch, 2008; Zamponi, 2008; Guises et al., 2009; Tighe et al., 2010; Fukumoto et al., 2013). This is because these properties are essential to a comprehensive understanding of the rheology of granular media. Therefore, it is also important to investigate the link between the initial packing and the following shear deformation of granular materials. For decades, many researchers have focused on the fabric evolution under shear to clarify this link (Bathurst and Rothenberg, 1989; Radjaï et al., 1998; Cambou et al., 2000; Hinrichsen anf Wolf, 2004; Snoeijer et al., 2006; O'Sullivan. 2011; Yun and Evans, 2011). Such works often deal with specimens which have different void ratios, i.e., loose, medium-dense and dense, and demonstrate the unique critical state that exists for granular materials. This fact is widely accepted by many researchers, especially in soil mechanics. However, there are few works focusing on specimens for which there is a difference in granular fabric at the initial state.

The focus of this study is to examine the effects of granular fabric on the shear behaviour. Numerical simulations of direct shear tests were performed based on the discrete element method (DEM) (Cundall and Strack, 1979). In order to prepare different specimens, two types of packing methods were employed; one specimen was generated by placing the particles geometrically, while the other specimen was generated by placing the particles randomly. As a result, two types of granular specimens were obtained with almost the same void ratio, but considerably different fabric. In a case like this, the effects of the fabric, which have a great influence on the yielding behaviour of granular soils, can be evaluated without concern for the void ratio.

Comparing the stress-strain responses obtained from the numerical simulation, it is revealed that the specimen in the case of the geometrical packing exhibits a higher peak shear stress ratio, while the specimen in the case of the random packing has no peak in shear stress. However, at a large shear strain, the values for shear stress and the average coordination number become constant; almost the same value is obtained for both samples.

Furthermore, the contact force distribution, the angular variation in contact forces, and the angular distribution of contact angles are chosen as the microscopic parameters to obtain a robust characterisation inside the granular soils. At the initial state, the two types of specimens have significantly different internal states associated with the different fabric. At the critical state, however, such differences gradually disappear with the increasing shear strain and a unique critical state is eventually achieved. The results revealed that not only macroscopic quantities, but also the contact force distribution and the angular variation in contact forces, have a unique critical state. In particular, the angular distribution of contact angles inside the shear band is also found to have a unique critical state.

The present paper is organized as follows. In Section 2, the numerical method, the system characteristics, and the loading parameters are firstly described. Details of the results of the numerical simulations and discussions are then given in Section 3. A summary is finally presented in Section 4.

2. SIMULATION DETAILS

2.1 Particle generation

Many techniques for particle packing have been proposed in DEM simulations. Previous research works have revealed that different packing methods have a strong influence on the arrangement of the particles (Rothenberg and Bathurst, 1992; Matuttis et al., 2000; Geng et al., 2001; Feng et al., 2003; Pöschel and Schwager, 2005; Abbireddy and Clayton, 2010; Fukumoto et al., 2013). In the present study, we choose two packing methods from among them in order to prepare different specimens which have different particle geometries; one specimen is generated by placing the particles geometrically, while the other specimen is generated by placing the particles randomly. After that, the granular samples are compressed by vertical stress, and then the two types of packings are obtained. In this paper, the former packing is called "geometric packing (GP)" and the latter one is called "random packing (RP)".

The process of particle generation for the GP method is illustrated in Figure 1 (a). The bottom-to-top reconstruction algorithm (Pöschel and Schwager, 2005) was employed to generate the particles geometrically in a rectangular area, 315 mm in width and 150 mm in height. In this system, each circular particle is supported by more than two contacts below their mass points. This geometric packing method is often used as it allows for the fast simulation of large static granular packings. The granular system consists of 11,082 particles, which have particle size distributions of D_{max}/D_{min} = 3, D_{max} = 3.0 mm, and D_{min} = 1.0 mm. Since the DEM calculation is not necessary for the GP method, the calculation time for the packing simulation is less than a minute when using CPU.

On the other hand, the process of particle generation for the RP method is illustrated in Figure 1 (b). Circular particles are randomly

placed in a rectangular box, 315 mm in width and 500 mm in height, while avoiding overlaps. In this generation process, the position of each particle is chosen randomly, one by one, and placed one by one in such a way that there are no overlaps with the particles which have already been placed. This granular system also consists of 11,082 particles, which are identical to those of the GP method. It should be noted here that, unlike the GP method, the RP method needs the DEM calculation. The calculation time for the packing simulation under the above condition is about 30 minutes when using CPU.

The density of the circular particles is 2600 kg/m^2. The contact springs, for both the particle-particle contacts and the particle-wall contacts, are assumed to be linear. The value for $k_n/\ k_t = 4$ ($k_n = 4.0\times10^7$ N/m and $k_t = 1.0\times10^7$ N/m), where k_n and k_t are the normal and the tangential spring constants, respectively. In addition, local non-viscous damping is introduced so that the equilibrium state can be achieved. The damping was constrained to be small enough so as not to have any effect on the results presented in this study. The value for the damping coefficient is 0.2.

A rolling friction model is also used here at the particle-particle contacts. This is because the rolling resistance of the particles plays an important role in the quasi-static behaviour of granular soils, which often consist of irregularly shaped particles (Iwashita and Oda, 1998; Tordesillas and Stuart, 2002; Lu and McDowell, 2007; Estrada et al., 2008; Matsushima and Chang, 2011; Fukumoto et al., 2013). The rolling friction model employed in this study is the same as that employed in our previous research (Fukumoto et al., 2013). At contacts between the wall and the particles, the rolling friction is set to zero for simplicity.

2.2 Direct shear simulation

After generating the specimens, the above-described material properties are set for all the particles. At the same time, the granular samples are then subjected to vertical compression by the top wall for stress control, in gravity. The constant confining stress acting on the top wall is 100 kN/m (i.e., the value of σ_v / k_n is 0.0025). This compression process is run until the variation in velocity of the upper wall is sufficiently small. The value for the average coordination number, *Z*, is determined by

$$Z = \frac{2M}{N}, \tag{1}$$

where *M* is the total number of contacts and *N* is the total number of particles in the contact network. The value for the void ratio, *e*, is defined by

$$e = \frac{V - V_p}{V_p}, \tag{2}$$

where V_p is the total volume of the particles and *V* is the total volume of the packing. The simulations are run with a time step of 2.0×10^{-6} s.

After the completion of compression, the particles near the top and bottom walls, coloured in black in Figure 1 (c), are fixed to model the rough surface boundaries. Then, direct shear tests are performed with a constant shear rate of 0.001 m /sec and a constant vertical pressure of 100 kN /m. In some preliminary simulations, it is observed that this shear rate ensured the quasi-static condition during testing (Zhang and Thornton, 2007). In the shearing process, the upper half of the box is displaced to the right, while the lower half of the box is fixed. The maximum shear displacement is 32 mm, which is about 10 percent of the width of the shear box.

The granular samples are sheared in a box, where the width, *L*, is 315 mm and the height, *H*, is about 150 mm (see Figure 1 (c)). Thus, the values for L/D_{max}, H/D_{max}, and L/H are 105, 50, and about 2, respectively. These values satisfy the conclusions of the previous research (Wang and Gutierrez, 2010), in which the effects of the specimen scale in the direct shear simulation were investigated.

In accordance with the above-described methods, a series of simulations is performed with several values for the sliding friction coefficient and the rolling friction coefficient in order to find the parameters which give a condition whereby the values for the void ratio are almost the same between the GP and the RP. In this process, the values for the sliding friction coefficient are set to be in the range of 0.3 to 0.6, while those for the rolling friction coefficient are set to be in the range of 0.05 to 0.20. As a result of trial and error, it is found that a sliding friction coefficient of 0.50 and a rolling friction coefficient of 0.10 are the best parameters for the purpose of the present research. Only the case for these parameters is discussed in the following section.

3. COMPARISON OF TWO TYPES OF SPECIMENS

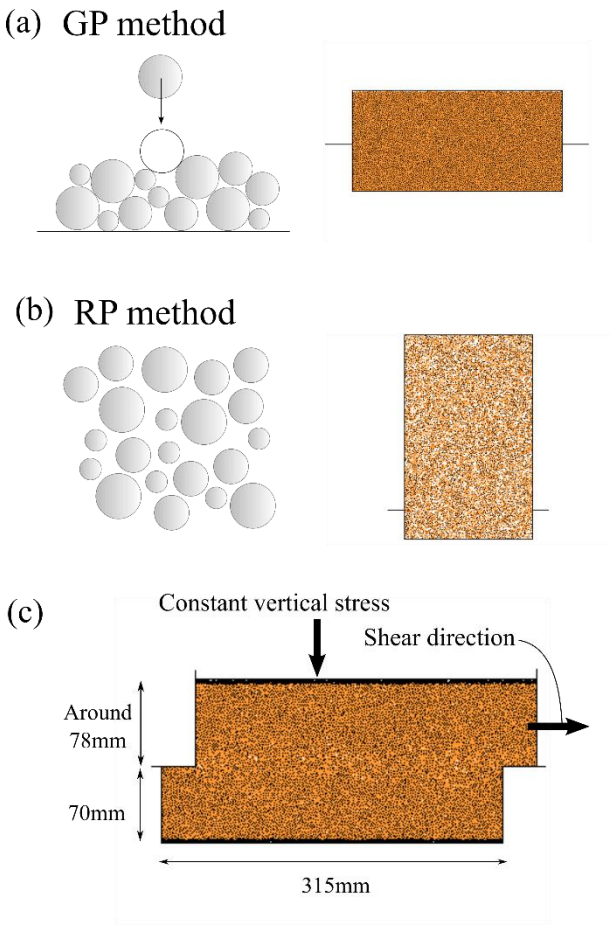

Figure 1 (a) Generation method of particles for GP method; (b) Generation method of particles for RP method; (c) Direct shear simulation

3.1 Initial state

In this subsection, we describe how the initial state under vertical confining stress before the shearing process is different for each specimen. The values for *Z* and *e* at this stable state are defined as Z_{ini} and e_{ini}. The value for Z_{ini} is 3.85 and that for e_{ini} is 0.236 in the GP, whereas the value for Z_{ini} is 3.36 and that for e_{ini} is 0.233 in the RP. In other words, the two granular samples have almost the same void ratios, but different average coordination numbers. From this data, it can be assumed that the microscopic properties of the two samples at the initial state are also distinct from each other.

At first, the contact force distributions of the two samples are compared. Figure 2 (a) shows the probability density distributions of the normal contact force, $P(f_n)$, for both the GP and the RP. The

normal contact forces are normalized by mean normal contact force $<f_n>$. From these shapes of $P(f_n)$, it can be observed that the plots for the RP show an upturn at very small forces near $f_n/<f_n>= 0$, but such an upturn can hardly be seen for the GP. This difference indicates that the fraction of the particle-particle contacts having small forces in the RP is larger than that in the GP. In other words, there are a lot of weakly supported particles in the RP. On the other hand, the plots for the GP have a clear peak at around $f_n/<f_n>= 1$, but no such peak is observed for the plots for the RP. This trend means that the GP has a more homogeneous stress distribution than the RP.

These trends in the contact force distributions in Figure 2 (a) can also be found in Figure 3, where the stress chains in a part of the granular samples at the initial state for both the GP and the RP are illustrated. The width of the line in the figures is proportional to the magnitude of the normal contact force. As can be seen from Figure 3, the stress chains in the GP are fine; they are distributed homogeneously. In the RP, however, the magnitude of the normal contact force varies widely and there are a lot of relatively large blanks inside the chains, i.e., inhomogeneous stress distributions can be observed.

Next, the angular variations in the normal contact forces between the two types of samples are compared, as detailed in Figure 2 (b). In this figure, 180 (deg.) is divided into 60 bins of 3 (deg.) each and the average normal contact force in each bin normalized by the mean normal force, $f_n(\theta)/< f_n >$, is plotted against the mean value of that bin. Contact angle θ is measured with respect to the horizontal axis in a counterclockwise direction. Previous studies have shown that this angular distribution is well fitted with just one parameter by Fourier series expressions in sheared granular assemblies (Bathurst and Rothenburg, 1989; Radjaï et al., 1998; Majmudar and Behringer, 2005; Snoeijer et al., 2006; Fukumoto et al., 2013). According to our previous studies (Fukumoto et al., 2013), the data are fitted by the solid curves drawn in Figure 2 (b) and described by the following equation:

$$\frac{f_n(\theta)}{< f_n >} = 1 - A\cos 2(\theta - \theta_f), \qquad \theta \in [0,180), \tag{3}$$

where A and θ_f are the fitting parameters which determine a wave pattern. The value for A corresponds to the amplitude of this wave-like distribution; it is the magnitude of mechanical anisotropy. The value for θ_f corresponds to the direction of the principal stress. The value for A in the GP is 0.46 and that in the RP is 0.39, while the values for θ_f are almost zero in both samples. At the initial state, the mechanical anisotropy along the direction of the vertical compression (i.e., $\theta_f = 0$) in the GP is slightly larger than that in the RP.

Finally, we compare the granular fabric between the two samples, as illustrated in Figure 2 (c). These polar diagrams display the distributions of the contact angles, $M(\theta)$, where contact angle θ is measured in the same manner as in Figure 2 (b). The GP has a lot of contacts around θ = 45 and 135 because of the peculiar particle geometry resulting from the GP method illustrated in Figure 1 (a). In the RP, where gravitational packing is executed, the contacts along the direction of gravity (θ=90) are larger than those in other directions.

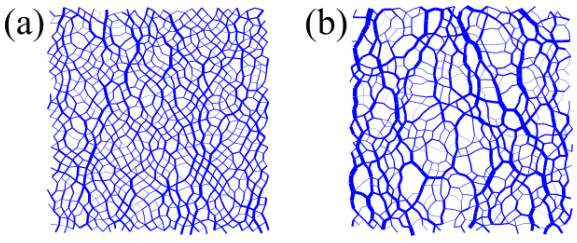

Figure 3 Stress chains in part of granular specimens at initial state
(a) For GP; (b) For RP

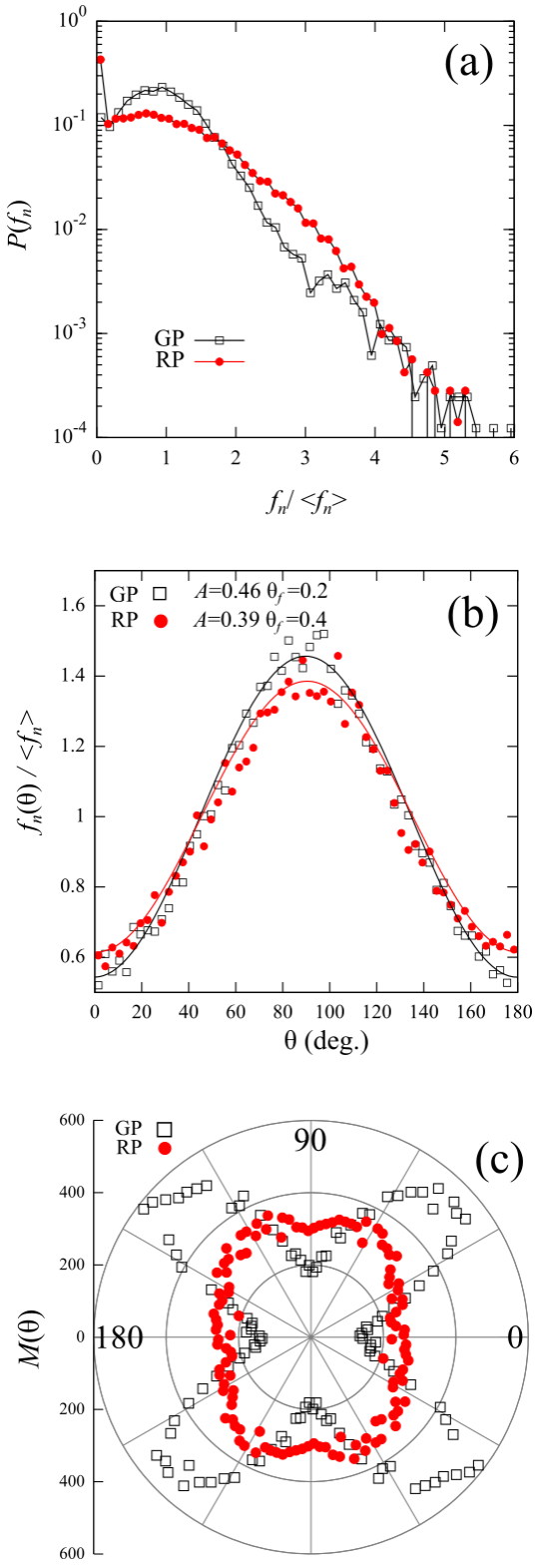

Figure 2 Stress state and fabric at initial state under vertical compression for GP and RP. (a) Probability density distributions of normal contact force; (b) Angular variation in normal contact forces; (c) Angular distribution of contact angles

From the above discussions, the two types of granular samples can be obtained. The values for the void ratio are almost the same, but the microscopic properties associated with the particle geometry are considerably different from each other. In such a case, the effects of the granular fabric, which have a great influence on the

yielding behaviour of granular soils, can be evaluated without concern for the void ratio.

3.2 Shear behaviour

Next, the present investigation is focused on how the shear behaviour of the two samples exhibit different trends. From the macroscopic point of view, shear stress ratio τ/σ_v and volumetric strain ε_v are plotted against applied shear strain γ, as shown in Figures 4 (a) and (b), respectively. The volumetric strain is evaluated based on the displacement of the upper wall, while the shear strain is evaluated based on the displacement of the side wall. The value for τ is the shear stress, while that for σ_v is the vertical stress. In addition, the evolution of the average coordination number, Z, and the average coordination number in the middle layer of the shear box, Z_{mid}, is also investigated, as detailed in Figures 5 (a) and (b).

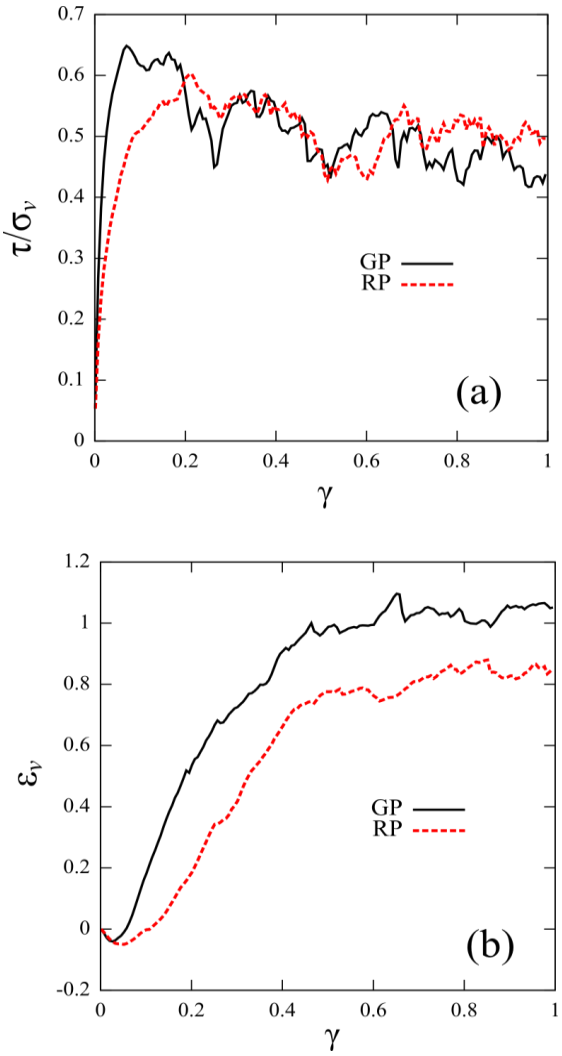

Figure 4 Bulk shear behavior for GP (solid line) and RP (dotted line). (a) Evolution of shear stress ratio τ/σ_v as function of shear strain γ; (b) Evolution of volumetric strain ε_v as function of shear strain γ

The shear strength is generally described by the peak shear stress ratio, τ/σ_v, which mainly depends on the void ratio. Here, the two samples have almost the same void ratio at the initial state before shear strain is applied, as described in Section 3.1. However, comparing the evolution of shear stress ratio τ/σ_v as a function of shear strain γ in Figure 4 (a), it is revealed that the specimen in the GP exhibits a higher peak at around $\gamma = 0.1$, but the specimen in the RP shows no clear peak in stress ratio. After the peak shear strength, at a large shear strain ($\gamma > 0.5$), the values for τ/σ_v become constant and they attain almost the same values for both the GP and the RP; that is, a critical state shear strength is observed. These observations mean that the shear strength of granular soils depends not only on the void ratio, but also on other factors, such as the coordination number, the stress state, and the particle orientation. In particular, it can be assumed that the homogeneity of the stress distribution is also closely related to the shear strength.

On the other hand, the evolution of volumetric strain σ_v, as a function of shear strain γ, is shown in Figure 4 (b), where negative values mean compression. In each case, the initial compression regime is followed by dilation until a steady state regime (around $\gamma = 0.5$) is reached, where the void ratio is almost constant and there is a weak tendency towards further dilation. In addition, it can be observed that the dilation in the RP occurs later than that in the GP. From the aspect of the stress-dilatancy relation (De Josselin de Jong, G., 1976), this dilation behaviour is consistent with the shear stress ratio curve given in Figure 4 (a). It should be noted here that, in terms of these macroscopic shear responses, it seems that the granular samples reach the critical state at around $\gamma = 0.5$.

Then, the evolution of average coordination number Z, as a function of shear strain γ, is addressed in Figure 5 (a). The value for Z in the GP decreases with an increase in γ until a constant value is attained at around $\gamma = 0.2$. In the RP, the evolution of Z shows the same trend, i.e., the value for Z reaches a constant value at a large shear strain. However, there is a difference in these constant values for Z between the GP and the RP. This is because the specimens in the shear box are not uniformly deformed. In general, the shear deformation becomes localized within the shear band with the progression of failure (Zhang and Thornton, 2007; Wang and Gutierrez, 2010). In particular, when a sufficient shear box scale is employed, such as in this study, a shear band forms in the narrow range of the middle layer of the specimen (Zhang and Thornton, 2007; Wang and Gutierrez, 2010).

For this reason, focus is also placed on the coordination number in the middle layer of the shear box, Z_{mid}, as shown in Figure 5 (b). The middle layer indicates the area of the shear box within a range of 55 mm to 85 mm in height. Coordination number Z_{mid} in the GP shows a rapid drop from the initial value, which is different from that in the RP, to constant values at $\gamma = 0.1$, that are almost the same as the RP. This constant value for Z_{mid} is smaller than that for Z. This observation indicates that the decrease in the coordination number in the middle layer is larger than that in the entire sample since the deformation has localized in the middle layer of the specimen. Furthermore, this rapid decrease in Z_{mid}, until $\gamma = 0.1$, implies that the microscopic properties considered in this study also undergo a dramatic change in this range of γ.

3.3 Critical state

In this subsection, the critical state of the two types of samples is discussed. The critical state is defined as the state at $\gamma = 1.0$ in the following discussions. Figures 6 (a), (b), and (c) show the stress state and the fabric at the critical state for the GP and the RP. As can be seen from Figure 6 (a), where the probability density distributions of the normal contact forces are plotted, the shape of $P(f_n)$ for the GP is consistent with that for the RP, although the shapes of $P(f_n)$ for the two specimens in the initial state are significantly different. In the critical state, the shapes of $P(f_n)$ change to the exponential form, while the curvature is observed in the initial state, as shown in Figure 2 (a). Previous research (Majmudar and Behringer, 2005) has also observed this transformation of $P(f_n)$ due to shear deformation.

Then, Figure 6 (b) shows the angular variation in the normal contact forces. This angular distribution is fitted with Equation (3) in the same manner as Figure 2 (b), and parameters A and θ_f are

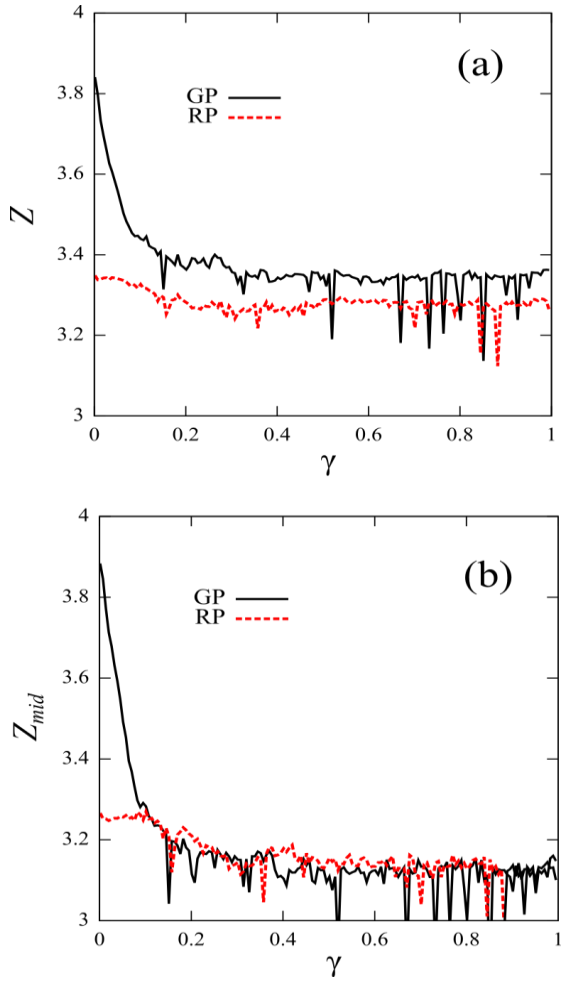

Figure 5 (a) Evolution of average coordination number Z as function of shear strain γ for GP (solid line) and RP (dotted line); (b) Evolution of average coordination number in middle layer of shear box Z_{mid} as function of shear strain γ

obtained. The value for A in the GP is 0.34, while that in the RP is 0.33, and the value for θ_f in the GP is 41.4, while that in the RP is 42.5. Compared to the initial state, the values for θ_f increase from nearly zero to 41.4 or 42.5. This is because the direction of the principal stress rotated in the shearing process. It can be concluded from this figure that the angular variations in the normal contact forces for the GP and the RP in the critical state are also almost consistent with each other.

These trends in the stress distribution in Figures 6 (a) and (b) can be also found in Figure 7, where the stress chains in a part of the granular samples at the critical state for the GP and the RP are illustrated. The contrast between the strong contact forces and the weak forces become clear through the shear deformation. The direction in which the strong contact force developed corresponds to the direction of the major principal stress.

Finally, we investigate the angular distribution of the contact angles for the GP and the RP, as shown in Figure 6 (c). As compared to Figure 2 (c), the number of contacts decreases along the direction of the minor principal stress. On the other hand, the reduction in the number of contacts along the direction of the major principal stress is small. As discussed above, in the critical state, the stress distribution and its angular variation are similar for each sample, but these polar diagrams are not completely consistent with each other. It seems that this is mainly because the shear deformation becomes localized within the shear band. The obtained results support the discussions on the evolution of the average coordination number.

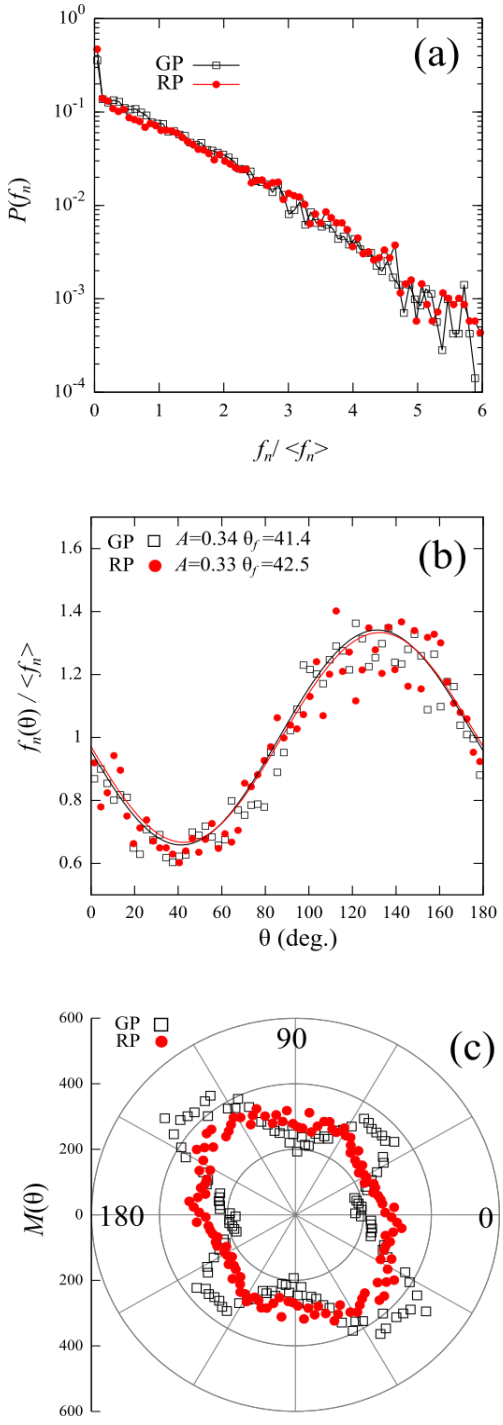

Figure 6 Stress state and fabric at critical state (γ = 1.0) for GP and RP. (a) Probability density distributions of normal contact force; (b) Angular variation in normal contact forces; (c) Angular distribution of contact angles

For this reason, focus is placed on the angular distribution of the contact angles in the middle layer of the shear box, $M_{mid}(\theta)$. Figures 8 (a) and (b) illustrate $M_{mid}(\theta)$ in the initial state (γ = 0.0) and in the critical state (γ = 1.0), respectively. Comparing Figure 8 (a) and Figure 2 (c), the distribution of $M_{mid}(\theta)$ is almost similar to that of $M(\theta)$ in the initial state. With increases in shear strain, it can be clearly seen from the figures that the difference in the shape of $M_{mid}(\theta)$, between the GP and the RP in the initial state, has disappeared and that they reach the same critical state.

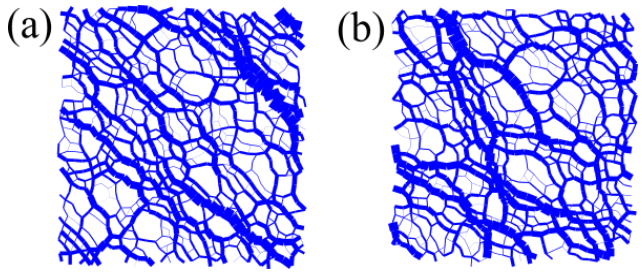

Figure 7 Stress chains in part of granular specimens at critical state (γ = 1.0). (a) For GP. (b) For RP

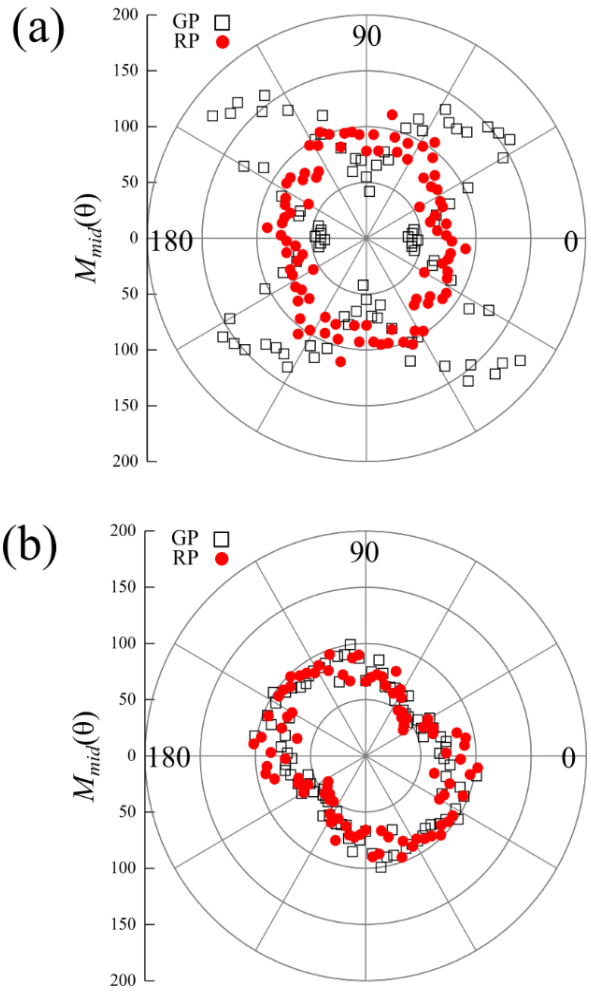

Figure 8 Angular distribution of contact angles in middle layer for GP and RP
(a) At initial state (γ = 0.0); (b) At critical state (γ = 1.0)

Previous studies have shown that there exists a unique critical state for granular materials in terms of the shear stress ratio. Such works deal with specimens which have different void ratios, i.e., loose, medium-dense, and dense. On the basis of these findings, the present study deals with the specimens which have different fabric and demonstrates that the initial microscopic properties, such as the contact force distribution, the angular variation in contact forces, and the angular distribution of contact angles, also develop under shear and eventually achieve a unique critical state.

3.4 Evolution of microscopic properties

Figure 9 shows the evolution of the stress state and the fabric under shear for the GP and the RP at γ= 0.05, γ = 0.10, and γ = 0.50. Focus is placed on the states at γ = 0.05 and γ = 0.10 because the microscopic properties may rapidly change after the beginning of the shearing process, as discussed in Section 3.2. Additionally, focus is also placed on the state at γ = 0.50 where the shear stress ratio and the volumetric strain become nearly constant, as shown in Figures 4 (a) and (b). The graphs in Figure 9 are plotted in the same manner as in Figures 2 and 6.

Firstly, the contact force distribution at various shear strain is discussed. It should be noted here that, as previously mentioned, there are substantial differences in the shape of $P(f_n)$ at the initial state between the GP and the RP. From Figure 9 (a), it seems that such differences have already disappeared at γ= 0.05 and that they have begun to form almost the same shape. However, paying careful attention to the range in $f_n / \langle f_n \rangle > 3$, the tail of $P(f_n)$ in the RP is seen to be located slightly superior to that in the GP. This tendency is still observed at γ= 0.10, as plotted in Figure 9 (b). As the shear strain increases, from Figure 9 (c), the GP and the RP are seen to achieve almost the same shapes of $P(f_n)$; they are characterized in exponential form.

Then, the evolution of the angular variation in the normal contact forces is considered. From Figure 9 (a), at γ = 0.05, the wave patterns are distinct from each other. In other words, the values for both A and θ_f in the GP are larger than those in the RP. Although similar shapes are obtained for $P(f_n)$ at γ = 0.05, the wave patterns are still significantly different at this point in time. From Figure 9 (b), at γ = 0.10, the gaps in A and θ_f decrease, and especially the value for θ_f in the RP is close to that in the GP. These results mean that the magnitude of anisotropy is still slightly different at γ = 0.10, but that the direction of the principal stress is almost the same. From Figure 9 (c), at γ = 0.50, the gaps in A and θ_f additionally decrease and approach the state at γ = 1.0, as shown in Figure 6 (b).

Finally, the evolution of the angular distribution of the contact angles in the middle layer of the shear box is discussed. From Figures 9 (a) and (b), the initial difference in the polar diagrams remains until γ = 0.10. From Figure 9 (c), the GP and the RP are seen to acquire similar angular distributions at γ = 0.50 with increases in the shear strain. In comparison with Figure 5 (b), it can be observed that the timing when similar contact orientations in the middle layer are obtained is later than the timing when similar coordination numbers in the middle layer are obtained. In fact, another researcher has also pointed out that the evolution towards the critical state value for the average coordination number is much faster than for the fabric anisotropy (Kruyt, 2012).

From the above discussions, it is shown that the contact force distribution, the angular variation in contact forces, and the angular distribution of contact angles have a unique critical state, respectively, and reach the critical state at a large shear strain (γ = 0.50), where the shear stress ratio and the volumetric strain become nearly constant. This fact implies that the critical state can be evaluated not only from the macroscopic perspective, but also from the aspect of microscopic properties.

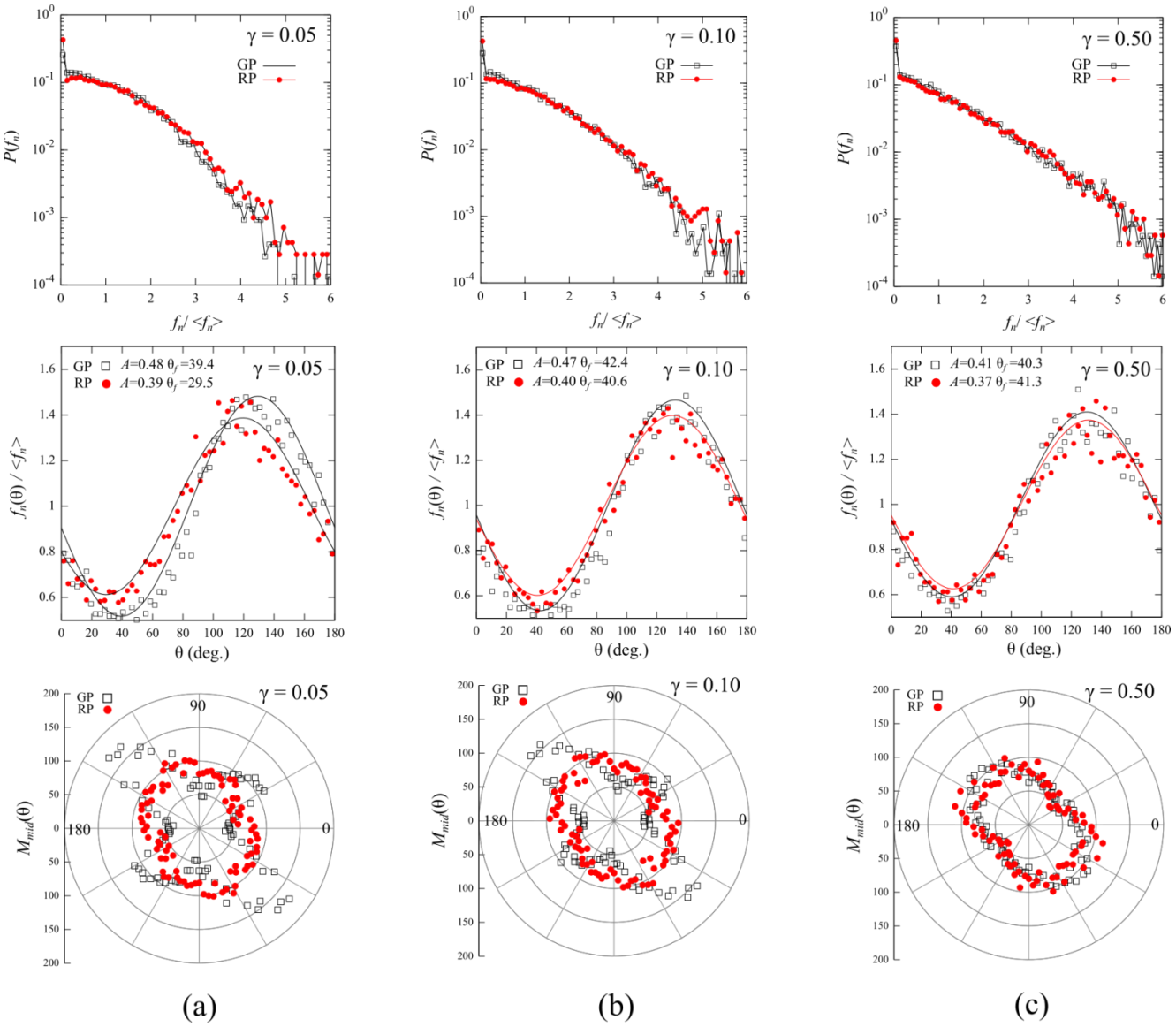

Figure 9 Evolution of probability density distributions of normal contact force, angular variation in normal contact forces, and angular distribution of contact angles under shear for GP and RP
(a) At γ = 0.05; (b) At γ = 0.10; (c) At γ = 0.50

4. CONCLUSIONS

In the present study, a comparison of sheared granular materials has been performed between two types of specimens, which have almost the same void ratio but considerably different fabric, by using DEM simulations of direct shear tests. Comparing the macroscopic shear responses, it has been shown that the shear strength of granular soils depends not only on the void ratio, but also on other factors, such as the coordination number, the stress state, and the particle orientation.

In addition to such macroscopic aspects, the contact force distribution, the angular variation in contact forces, and the angular distribution of contact angles were chosen as the microscopic parameters to obtain a robust characterisation inside the granular soils, and the evolution of such microscopic properties under the shearing process were investigated. The results revealed that not only macroscopic quantities, but also the contact force distribution and the angular variation in contact forces, have a unique critical state, where the shape of $P(f_n)$ is exponential and the wave pattern of $f_n(\theta)/< f_n >$ is consistent with the direction of the principal stress. In particular, the polar diagram of $M_{mid}(\theta)$ inside the shear band was also found to have a unique critical state.

Since this study has dealt with just two packing methods, for the sake of simplicity, the obtained results cannot be extended to a comprehensive understanding of sheared granular soils. Therefore, further studies, which treat various packing conditions, are needed in the future.

5. ACKNOWLEDGEMENTS

This work was supported by JSPS KAKENHI, Grant-in-Aid for Young Scientists (B), Grant number 16K18146.

6. REFERENCES

Abbireddy, C. O. R. and Clayton, C. R. I. (2010) "Varying initial void ratios for DEM simulations." Géotechnique, 60, Issue 6, pp 497-502.

Bathurst, R. J. and Rothenburg, L. (1998) "Observation on stress-force fabric relationships in idealized granular materials". Géotechnique, 39, Issue 4, pp 601-614.

Cambou, B., Chaze, M. and Dedecker, F. (2000) "Change of scale in granular materials". European Journal of Mechanics A-Solids, 19, pp 999-1014.

Cundall, P.A. and Strack, O.D.L. (1979) "A discrete numerical model for granular assemblies". Géotechnique, 29, Issue 1, pp 47-65.

De Josselin de Jong, G. (1976) "Rowe's stress-dilatancy relation based on friction". Géotechnique, 26, Issue 3, pp 527-534.

Estrada, N., Taboada, A. and Radjaï, F. (2008) "Shear strength and force transmission in granular media with rolling resistance". Physical Review E, 78, Issue 6, 021301.

Feng, Y., Han, K. and Owen, D. (2003) "Filling domains with disks: An advancing front approach". International Journal of Numerical Methods in Engineering, 56, Issue 5, pp 699-731.

Fukumoto, Y., Sakaguchi, H. and Murakami, A. (2013). "The role of rolling friction in granular packing". Granular Matter, 15, Issue 2, pp 175-182.

Geng, J., Longhi, E., Behringer R.P. and Howell, D.W. (2001) "Memory in two-dimensional heap experiments". Physical Review E, 64, R060301.

Goldenberg, C. and Goldhirch, I. (2008) "Effects of friction and disorder on the quasistatic response of granular solids to a localized force". Physical Review E, 77, 041303.

Guises, R., Xiang, J., Latham J. P. and Munjiza, A. (2009) "Granular packing: numerical simulation and the characterisation of the effect of particle shape". Granular Matter, 11, pp 281-292.

Hinrichsen, W. and Wolf, D.E. (2004) "The physics of granular media". John Wiley & Sons., Weinheim.

Iwashita, K. and Oda, M. (1999) "Mechanics of granular materials: an introduction". A.A.Balkema, Rotterdam.

Jaeger, H., Nagel, S. and Behringer, R.P.（1996) "Granular solids, liquids, and gases". Reviews of Modern Physics, 68, Issue 4, 1259.

Kruyt, N. P. (2012) "Micromechanical study of fabric evolution in quasi-static deformation of granular materials". Mechanics of materials. 44, pp 120-129.

Lu, M. and McDowell, G.R. (2007) "The importance of modeling ballast particle shape in the discrete element method". Granular Matter, 9, pp 69-80.

Majmudar, T. S. and Behringer, R. P. (2005) "Contact force measurements and stress-induced anisotropy in granular materials", Nature, 435, 1079.

Makse, H. A., Johnson, D. L. and Schwartz, L. M. (2000) "Packing of Compressible Granular Materials". Physical Review Letter, 84, Issue 18, 4160.

Matuttis, H.G., Luding, S. and Herrmann, H.J. (2000) "Discrete element simulations of dense packings and heaps made of spherical and nonspherical particles". Powder Technology, 109, pp 278-292.

Matsushima, T. and Chang, C. S. (2011) "Quantitative evaluation of the effect of irregularly shaped particles in sheared granular assemblies". Granular Matter, 13, Issue 3, pp 269-276.

Mueth, D. M., Jaeger, H. M. and Nagel, S. R. (1998) "Force distribution in a granular medium". Physical Review E, 57, Issue 3, 3164.

O'Sullivan, C. (2011) "Particulate discrete element modelling: A geomechanics perspective". Taylor & Francis, New York.

Pöschel, T. and Schwager, T. (2005) "Computational Granular Dynamics". Springer, New York.

Radjaï, F., Wolf, D. E., Jean, M. and Moreau, J-J. (1998) "Bimodal Character of Stress Transmission in Granular Packing". Physical Review Letter, 80, Issue 1, 61.

Rothenberg, L. and Bathurst, R.J. (1992) "Micromechanical features of granular assemblies with planer elliptical particles". Géotechnique, 42, Issue 1, pp 79-95.

Roux, J. N. (2000) "Geometric origin of mechanical properties of granular materials ". Physical Review E, 61, Issue 6, 6802.

Snoeijer, J. H., Ellenbroek, W. G., Vlugt, T. J. H. and van Hecke, M. (2006) "Sheared Force Network: Anisotropies, Yielding, and Geometry", Physical Review Letter, 96, 098001.

Tighe, B. P., Snoeijer, J. H., Vlugt, T. J. H and van Hecke, M. (2010) "The force network ensemble for granular packings". Soft Matter, 6, pp 2908-2917

Tordesillas, A. and Stuart Walsh, D.C. (2002) "Incorporating rolling resistance and contact anisotropy in micromechanical models of granular media". Powder Technology, 124, pp 106-111.

Wang, J. and Gutierrez, M. (2010) "Discrete element simulations of direct shear specimen scale effects". Géotechnique, 60, Issue 5, pp 395-409.

Yun, T. S. and Evans, T. M. (2011) "Evolution of at-rest lateral stress for cemented sands: experimental and numerical investigation". Granular Matter, 13, Issue 5, pp 671-683.

Zamponi, F. (2008) "Mathematical physics: Packings close and loose". Nature, 453, Issues 7195, pp 606-607.

Zhang, L. and Thornton, C. (2007) "A numerical examination of the direct shear test". Géotechnique, 57, Issue 4, pp 343-354.